Scripta Materialia 148 (2018) 33–36

Contents lists available at ScienceDirect

Scripta Materialia

journal homepage: www.elsevier.com/locate/scriptamat

Regular article

Radiation resistance of oxide dispersion strengthened alloys: Perspectives from in situ observations and rate theory calculations

Xiang Liu [a,*], Yinbin Miao [b], Meimei Li [b], Marquis A. Kirk [b], Guangming Zhang [c], Shigeharu Ukai [d], Stuart A. Maloy [e], James F. Stubbins [a,f]

[a] Department of Nuclear, Plasma, and Radiological Engineering, University of Illinois at Urbana-Champaign, Urbana, IL 61801, USA
[b] Nuclear Engineering Division, Argonne National Laboratory, Lemont, IL 60439, USA
[c] Qingdao University of Technology, Qingdao, Shandong 266033, China
[d] Materials Science and Engineering, Faculty of Engineering, Hokkaido University, N13, W-8, Kita-ku, Sapporo, Hokkaido 060-8628, Japan
[e] Materials Science and Technology Division, Los Alamos National Laboratory, Los Alamos, NM 87545, USA
[f] International Institute for Carbon Neutral Energy Research (WPI-I2CNER), Kyushu University, 744 Motooka, Nishi-ku, Fukuoka 819-0395, Japan

ARTICLE INFO

Article history:
Received 21 November 2017
Received in revised form 9 January 2018
Accepted 15 January 2018
Available online xxxx

Keywords:
Oxide dispersion strengthened (ODS) alloy
Dislocation structure
Microstructure
Transmission electron microscopy
Radiation enhanced diffusion (RED)

ABSTRACT

Here, in situ ion irradiation and rate theory calculations were employed to directly compare the radiation resistance of an oxide dispersion strengthened alloy with that of a conventional ferritic/martensitic alloy. Compared to the rapid buildup of dislocation loops, loop growth, and formation of network dislocations in the conventional ferritic/martensitic alloy, the superior radiation resistance of the oxide dispersion strengthened alloy is manifested by its stable dislocation structure under the same irradiation conditions. The results are consistent with rate theory calculations, which show that high-density nanoparticles can significantly reduce freely migrating defects and suppress the buildup of clustered defects.

Advanced nuclear reactor systems with inherent safety features are being developed as reliable and sustainable clean energy sources. However, the harsh reactor environment, especially high-dose neutron irradiation (>100 dpa), rules out the extended use of most conventional structural materials. By introducing ultra-stable, high-density (~10^{23} n/m^3) dispersoids to suppress radiation-induced defect formation, nanostructured oxide dispersion strengthened (ODS) alloys represents one of the most promising candidate materials for structural applications in advanced reactors [1]. Commonly used dispersoids are Y-Ti-O nanoparticles (2–4 nm) in ODS Fe-Cr alloys and relatively coarse (~10 nm) Y-Al-O nanoparticles in ODS FeCrAl alloys [2–4]. The stability of these nanoparticles under irradiation or high temperature heat treatment has been demonstrated by several studies [5–12].

A previous review paper [1] compared the helium bubbles in ODS alloy MA957 versus the bubbles in reduced-activation martensitic alloys Eurofer97 and F82H, and found that the helium bubbles in irradiated ODS alloys tend to have higher number density and smaller size, which was also confirmed by a recent study [13]. It is suggested that the nanoparticles in ODS alloys help absorb helium atoms and protect the grain boundaries from helium embrittlement. These findings provide some ideas about the enhanced radiation resistance of ODS alloys. However, most existing studies rely on the ex situ irradiation data and often the comparisons could only be made on alloys with distinct chemical composition, heat treatment, initial microstructure, and irradiation history. Moreover, to the best of our knowledge, few data on the evolution of the dislocation structure, which is closed related to irradiation hardening, of ODS alloys versus non-ODS alloys under similar irradiation conditions could be found in literature.

To identify the differences in the radiation response, especially the evolution of the dislocation structure, bewteen ODS alloys and non-ODS alloys, this study employed in situ transmission electron microscopy (TEM) with concurrent ion irradiation so that a direct comparison of the microstructure changes in different alloy systems under the same exposure conditions is possible. The in situ capability also allows the dynamic observation of the microstructure evolution of exactly the same area over a range of dose levels. In this study, the comparison was made between a Fe-9Cr ODS ferritic/martensitic (F/M) alloy (designated 9CrODS) and a Fe-9Cr F/M alloy, T91. The 9Cr alloys belong to the high Cr alloy family that shows promising resistance to void swelling and irradiation creep [14]. Table 1 shows the nominal chemical composition of the as-received materials.

The as-received T91 and 9CrODS underwent similar heat treatment: T91 was normalized at 1037 °C for 1 h, air cooled, and then tempered at

* Corresponding author.
E-mail address: xliu128@illinois.edu (X. Liu).

https://doi.org/10.1016/j.scriptamat.2018.01.018
1359-6462/

Table 1
Nominal chemical composition of as-received T91 and 9CrODS alloys, in wt.%.

Alloy	Fe	Cr	C	Si	Mn	Ni	W	N	Mo	Nb	Ti	Y	O	Y_2O_3
T91	Bal.	9.24	0.089	0.28	0.47	0.16	–	0.035	0.96	0.054	0.002	–	0.008	–
9CrODS	Bal.	9.08	0.14	0.06	0.09	0.03	1.97	0.013	–	–	0.23	0.29	0.16	0.37

760 °C for 1 h and air cooled, and 9CrODS was normalized at 1050 °C for 1 h, air cooled, followed by tempering at 800 °C for 1 h and air cooled.

The in situ ion irradiation experiments were performed at the IVEM-Tandem facility, Argonne National Laboratory (ANL). The experimental setup was identical to the one previously described by Liu et al. [15]. A Hitachi 9000 NAR electron microscope operated at 200 kV was used for post-irradiation TEM imaging. The incident ion beam was 30° to the electron beam and on average ~15° to the foil normal. TEM thin foils were irradiated by 1 MeV Kr^{++} ions at 400 °C up to 4.2×10^{15} ions/cm^2, corresponding to 7.0 dpa under the Kinchin-Pease option using SRIM calculation with displacement energy set to 40 eV [16,17]. The ion flux was kept at 6.25×10^{11} ions/(cm^2·s), representing a dose rate of 1.0×10^{-3} dpa/s in the thin foil region and the Kr^{++} ions were sufficiently energetic to pass through the foil.

In order to make the comparison more reliable, martensite grains with similar initial line dislocation density (~1×10^{14} m^{-2}) in 9CrODS and T91 were chosen, and the TEM images were taken under similar kinematic diffraction conditions with $\mathbf{g}_{110}$ strongly excited. Fig. 1 shows the in situ TEM observations of the microstructure evolution of 9CrODS versus F/M steel T91. The results of T91 were previously described in detail by Liu et al. [15]. As can be seen from Fig. 1(a)–(e), the dislocation structure in 9CrODS is very stable even after being irradiated to 4.2×10^{15} ions/cm^2 (~7 dpa), as manifested by very low-density black-dot damage accumulation. Similar black-dot dislocation loops have also been reported in previous studies [18,19]. Both the dislocation loops and the Y-Ti-O nanoparticles can appear as dark spots in the bright-field images, but the dislocation loops are distinguishable from the nanoparticles as they appear as bright spots in the corresponding weak-beam dark-field images. One example of this imaging effect can be found in the Supplementary Material. In Fig. 1, several possible black-dot loops were marked by red arrows. The loops remained small black-dots (2–4 nm) and no loop growth was observed up to 7 dpa. Some changes did occur to the pre-existing dislocations, due to dislocation-defect interactions. In addition to the negligible amount of dislocation loops, post-irradiation examination (PIE) also did not find any resolvable voids.

In contrast, as shown in Fig. 1(f)–(j), T91 maintained relative stability only up to around 6.0×10^{14} ions/cm^2 (~1 dpa), and black-dot dislocation loops started to accumulate around 1.8×10^{15} ions/cm^2 (~3 dpa). The black-dot dislocation loops increased in size with increasing dose. One example of loop growth is the loop marked by red circle in Fig. 1 (i) and (j). Loops of 10–20 nm were commonly found after the sample was irradiated to 4.2×10^{15} ions/cm^2. In addition to the buildup of black-dot loops and loop growth, apparent dislocation segments also occurred around 3.0×10^{15} ions/cm^2 (~5 dpa). It is known that in F/M steels, the dislocation segments will evolve into network dislocations, which contribute to irradiation hardening by impeding dislocation motion as well as void swelling by preferentially absorbing interstitials (sink bias) in the high dose regime.

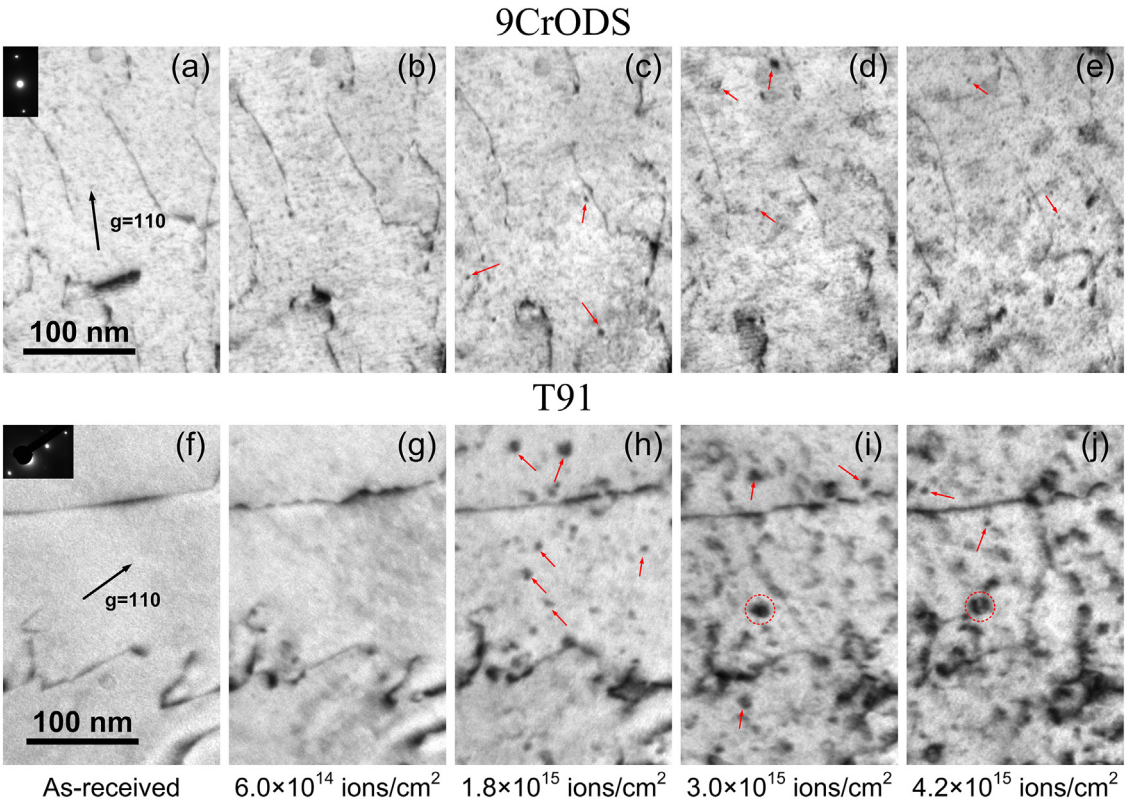

Fig. 1. In situ TEM observations of the microstructure evolution of (a)–(e) 9CrODS, and (f)–(j) F/M steel T91 at various dose levels. Both specimens were irradiated by 1.0 MeV Kr^{++} ions at 400 °C. The T91 result is from previous work [15].